N-terminal domain of human Hsp90 triggers binding to the cochaperone p23

G. Elif Karagöz[a,1], Afonso M. S. Duarte[a,1], Hans Ippel[b], Charlotte Uetrecht[c,d], Tessa Sinnige[a], Martijn van Rosmalen[a], Jens Hausmann[a,2], Albert J. R. Heck[c,d], Rolf Boelens[b], and Stefan G. D. Rüdiger[a,3]

[a]Cellular Protein Chemistry, Bijvoet Center for Biomolecular Research, Utrecht University, Padualaan 8, 3584 CH Utrecht, The Netherlands; [b]Biomolecular NMR Spectroscopy, Bijvoet Center for Biomolecular Research, Utrecht University, Padualaan 8, 3584 CH Utrecht, The Netherlands; [c]Biomolecular Mass Spectrometry and Proteomics Group, Bijvoet Center for Biomolecular Research and Utrecht Institute for Pharmaceutical Sciences, Utrecht University, Padualaan 8, 3584 CH Utrecht, The Netherlands; and [d]Netherlands Proteomics Centre, Padualaan 8, 3584 CH Utrecht, The Netherlands

Edited by Susan Lindquist, Whitehead Institute for Biomedical Research, Cambridge, MA, and approved November 16, 2010 (received for review August 12, 2010)

The molecular chaperone Hsp90 is a protein folding machine that is conserved from bacteria to man. Human, cytosolic Hsp90 is dedicated to folding of chiefly signal transduction components. The chaperoning mechanism of Hsp90 is controlled by ATP and various cochaperones, but is poorly understood and controversial. Here, we characterized the Apo and ATP states of the 170-kDa human Hsp90 full-length protein by NMR spectroscopy in solution, and we elucidated the mechanism of the inhibition of its ATPase by its cochaperone p23. We assigned isoleucine side chains of Hsp90 via specific isotope labeling of their δ-methyl groups, which allowed the NMR analysis of the full-length protein. We found that ATP caused exclusively local changes in Hsp90's N-terminal nucleotide-binding domain. Native mass spectrometry showed that Hsp90 and p23 form a 2:2 complex via a positively cooperative mechanism. Despite this stoichiometry, NMR data indicated that the complex was not fully symmetric. The p23-dependent NMR shifts mapped to both the lid and the adenine end of Hsp90's ATP binding pocket, but also to large parts of the middle domain. Shifts distant from the p23 binding site reflect p23-induced conformational changes in Hsp90. Together, we conclude that it is Hsp90's nucleotide-binding domain that triggers the formation of the $Hsp90_2p23_2$ complex. We anticipate that our NMR approach has significant impact on future studies of full-length Hsp90 with cofactors and substrates, but also for the development of Hsp90 inhibiting anticancer drugs.

methyl-transverse-relaxation optimized spectroscopy | protein–protein interactions | heat shock proteins | asymmetry | allostery

Hsp90 chaperones are dimeric protein machines that assist the folding and maturation of signal transduction compounds by shuttling between open and closed conformations in a nucleotide-dependent manner (1–9). The overall structure of the Hsp90 machine is conserved, but the conformational variation is remarkable between Hsp90 homologues in different cellular compartments and species. Even more striking is the observation that the same nucleotide state differs in its ratio of open to closed conformation between homologues (10).

Eukaryotic cytosolic Hsp90s are regulated by a large variety of cofactors, which may influence Hsp90's shuttling between open and closed states (1). The ATP state of Hsp90 is stabilized by the cochaperone p23 (11). The stoichiometry of the Hsp90-p23 complex is controversial and might differ between, e.g., human and yeast Hsp90 (12, 13). Although the crystal structure of the yeast homologues of Hsp90 and p23 ($Sba1^{p23}$) revealed a 2:2 complex (11), isothermal titration calorimetry (ITC) and CD measurements resulted in conflicting interpretations whether one or two $Sba1^{p23}$ molecules may bind to an Hsp90 dimer (12, 14).

NMR spectroscopy is a powerful method to reveal high resolution structural information on proteins in solution and allowed structural insights into the allosteric mechanisms of, e.g., Hsp70 chaperones (15, 16). NMR studies of isolated domains of Hsp90 elucidated interactions with nucleotides, drugs and cochaperones (17–21). Conventional NMR methods, however, are restricted to proteins of up to 50 kDa. Complexes of full-length Hsp90 with cofactors are around 200 kDa, and only studies with the entire protein would allow for dynamic insights that take Hsp90's extensive dimeric domain–domain interactions into account. Some of us have previously analyzed Hsp90 binding to a substrate using advanced NMR techniques, but at that time assignment of Hsp90 resonances was impossible (22). The Kay laboratory recently pioneered NMR spectroscopy for large proteins by specific labeling of methyl groups of aliphatic amino acids, including isoleucine (Ile), to overcome some of those limitations (23, 24). For large proteins, proton–carbon spectra of those methyl groups result in significantly higher intensity and resolution compared to proton–nitrogen spectra.

Here, we have elucidated the nature of the human Hsp90-p23 complex in solution by using NMR spectroscopy and native mass spectrometry. We revealed mechanistic insights in the allosteric regulation of Hsp90 by p23 using a four-step strategy: (*i*) overcoming the NMR size limit for large protein complexes by using an Ile labeling strategy, (*ii*) NMR assignment of isoleucine resonances in the smaller, isolated domains of Hsp90 domains and transferring these assignments onto the spectrum of full-length Hsp90, (*iii*) mapping the chemical shift perturbation of full-length Hsp90 induced by ATP binding, and (*iv*) monitoring of p23 binding to a full-length Hsp90-ATP complex by NMR spectroscopy and native mass spectrometry.

Assignment Strategy for NMR of Hsp90

We noted that Iles are well spread over the entire Hsp90 molecule and are represented in every crucial region (Fig. 1*A*). For that reason we specifically ^{13}C- and ^{1}H-labeled the δ-methyl group of all Ile side chains in an otherwise deuterated protein to obtain high-resolution signals throughout the protein. We acquired methyl-transverse-relaxation optimized spectroscopy (TROSY) proton–carbon spectra of methyl Ile labeled Hsp90. We detected 45 out of 48 possible peaks (Fig. 1*B*). Hsp90 is rather a challenging protein for NMR studies not only due to its size but also due to the presence of several disordered regions. The simultaneous

Author contributions: G.E.K., A.M.S.D., A.J.R.H., R.B., and S.G.D.R. designed research; G.E.K., A.M.S.D., H.I., C.U., T.S., M.v.R., and J.H. performed research; G.E.K., A.M.S.D., H.I., C.U., A.J.R.H., R.B., and S.G.D.R. analyzed data; and G.E.K., A.M.S.D., and S.G.D.R. wrote the paper.

The authors declare no conflict of interest.

This article is a PNAS Direct Submission.

[1]G.E.K. and A.M.S.D. contributed equally to this work.

[2]Present address: Division of Biochemistry, Netherlands Cancer Institute, Plesmanlaan, 121, 1066 CX Amsterdam, The Netherlands.

[3]To whom correspondence should be addressed. E-mail: s.g.d.rudiger@uu.nl.

This article contains supporting information online at www.pnas.org/lookup/suppl/doi:10.1073/pnas.1011867108/-/DCSupplemental.

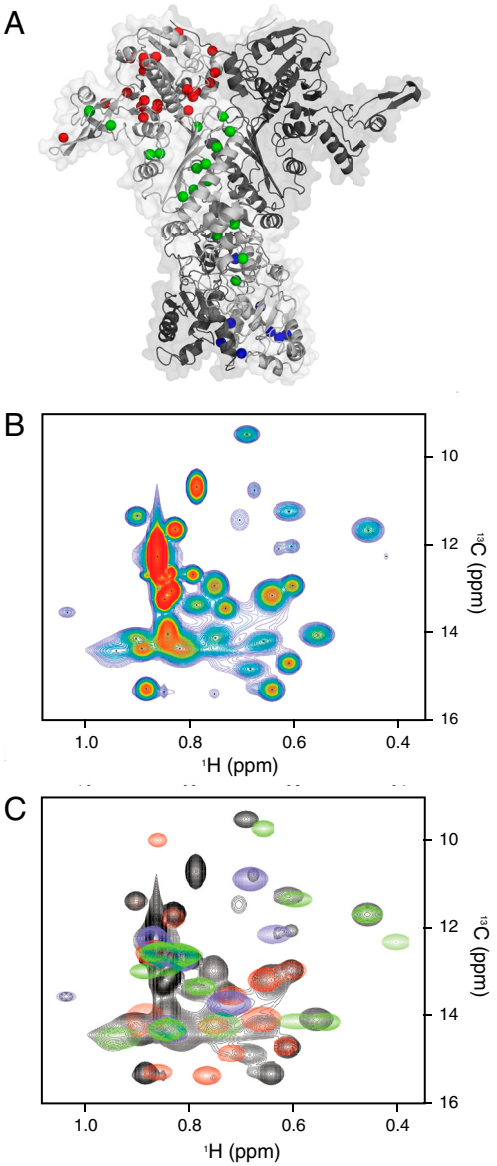

Fig. 1. Isoleucines are ubiquitous markers for NMR analysis of Hsp90. (*A*) Homology model of human Hsp90 with Ile side chains depicted in red (Hsp90-N), green (Hsp90-M), and blue (Hsp90-C) in one monomer. Hsp90 monomers are shown in two shades of gray. (*B*) Rainbow representation of ^{1}H-^{13}C-Ile methyl-TROSY cross-peaks of full-length Hsp90, colored from blue to red according to relative intensities. The centers of 34 peaks are indicated by black dots. (*C*) Hsp90's Ile side chains can be assigned via spectra of the individual domains. Overlay of full-length Hsp90 methyl-TROSY spectrum of Iles with spectra of the individual domains (full-length Hsp90, black; Hsp90-N, red; Hsp90-M, green; Hsp90-C, blue).

presence of dynamic regions and rigid segments resulted in signals of diverse intensity and linewidth (Fig. 1*B*).

The assignment of the peaks of the full-length protein is essential for monitoring conformational changes and the mapping of binding sites of cofactors. At present, an NMR assignment of the full-length Hsp90 protein is still impossible. To circumvent the problems associated with the size of Hsp90, we compared the Ile methyl-TROSY spectra of the isolated N-terminal, middle, and C-terminal domains (Hsp90-N, Hsp90-M, and Hsp90-C) to spectra of the full-length protein. Most of the peaks in the spectra of full-length Hsp90 could be assigned to one of the three individual domains (Fig. 1*C*, Fig. S1, and Table S1).

We conclude that, in solution, full-length Hsp90 behaves similar to the sum of its individual domains. We assigned all Ile side chains of Hsp90-N and most of Hsp90-M. Once we assigned the Ile spectra of those domains, we could readily transfer them to the NMR spectra of full-length Hsp90. The signals that can be clearly annotated provide markers that allowed probing potential conformational movements under catalytic turnover conditions in Hsp90's key regions.

ATP-Dependent Changes Are Restricted to the N-Terminal Domain

We acquired NMR spectra of full-length Hsp90 with and without ATP (Figs. 1*B* and 2*A*). We generated ATP-bound Hsp90 either by using the "nonhydrolysable" analogues AMP-PNP and ATPγS or by using an ATP-regenerating system. Because we found some Hsp90-independent decay of AMP-PNP under our experimental conditions by ^{31}P-NMR, we preferred the ATP-regenerating system to create Hsp90-ATP complexes, which were stable for more than 4 h. ATP hydrolysis (7×10^{-5} s^{-1}) is significantly slower than dissociation of ADP (3 s^{-1}), whereas binding of ATP is fast (1×10^{5} M^{-1} s^{-1}) (25). In the presence of the ATP-regenerating system, Hsp90 is therefore fully loaded with ATP. We did not observe significant differences in the NMR spectra of ATP and AMP-PNP loaded Hsp90; thus, we conclude that both represent the ATP state of Hsp90.

ATP-dependent peak shifts mapped to a subset of Iles in Hsp90-N consisting mainly of residues that either belonged to the ATP binding pocket and/or its lid (Ile53, Ile75, Ile90, and Ile122) or to the helical region required for N-terminal dimerization (Ile20, Ile27, and Ile28; Fig. 2 *B* and *C* and Figs. S2*A* and S3*A*). We observed similar shifts in the isolated Hsp90 upon binding of AMP-PNP (Fig. S4). Our data indicate that monitoring of chemical shifts of Ile side chains allows mapping of specific ligand binding to full-length Hsp90.

We noted that the methyl resonance corresponding to Ile90 was split into two signals, in addition to the chemical shift change upon ATP binding. This effect was restricted to the spectra of Hsp90 full length; we did not observe this for Hsp90-N (Fig. S4). In the homology model of human Hsp90, the δ-carbon atom of Ile90 at the distal end of the ATP binding pocket is 7 Å away from the adenine ring of the ATP, in the direction of the ring plane (Fig. S5*A*). Interestingly, despite this significant distance there are no residues that would occupy the space between Ile90 and ATP, in neither the homology model nor the crystal structure of the yeast homologues nor crystal structures of human Hsp90-N (11, 26). In a crystal structure of human Hsp90-N this Ile is rotated by 90° away from the center of the nucleotide-binding pocket when unoccupied, increasing the distance from the nucleotide by further 2 Å (26). Splitted resonance peaks of Ile90 may reflect the potential structural plasticity on this side of the pocket after binding of ATP.

We could not allocate significant chemical shifts to Iles of the middle and C-terminal domains of full-length Hsp90. We concluded that ATP did not induce global conformational changes within those domains. This indicates that ATP-induced dimerization of the N-terminal domains is determined by changes in Hsp90-N and does not lead to structural changes in Hsp90-M and Hsp90-C.

The Cochaperone p23 Changes the Environment of Hsp90-Bound ATP

The NMR approach provided us with an allosteric fingerprint of different, essential conformational steps of the Hsp90 ATPase cycle. We applied this now for monitoring binding of the cochaperone p23 to Hsp90. Native mass spectrometry indicated that ATP is required for efficient interaction of these two proteins. We observed that free Hsp90 was the main species at 2:3 Hsp90:p23 (monomer concentration) in the absence of ATP and Mg^{2+} and only minor signals were found that corresponded to 2:1 Hsp90-p23 complexes (Fig. 4*C*). Initial NMR experiments also

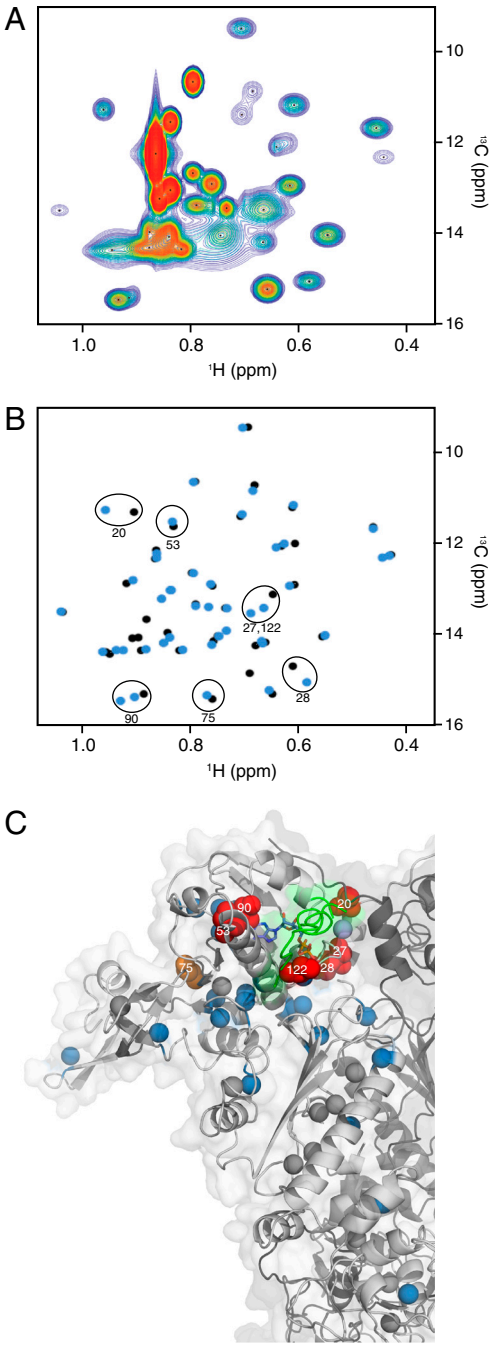

Fig. 2. ATP induces conformational changes in the Hsp90 N-terminal domain. (*A*) Rainbow representation of ^{1}H-^{13}C-Ile methyl-TROSY cross-peaks of full-length Hsp90 with ATP. The centers of 34 peaks are indicated by black dots. (*B*) Overlay of Hsp90 Ile methyl-TROSY spectra in absence (black) and presence of ATP (blue) shown as a peak position plot. The isoleucines showing significant shift are indicated and encircled [combined chemical shift difference $\Delta\nu = ((0.25\Delta\nu_C)^2 + \Delta\nu_H{}^2)^{1/2}$, Ile residues with $\Delta\nu > 0.015$ ppm are encircled]. (*C*) Ile side chains shifting upon ATP binding, plotted on one monomer of the homology model of the Hsp90 structure. Depicted are Ile side chains shifting upon ATP binding (Iles with $0.015 > \Delta\nu > 0.02$ are shown as orange spheres, Ile with $\Delta\nu > 0.02$ as red spheres), Ile methyl groups that do not shift (blue spheres), and Ile methyl groups that either could not be assigned or for which results were inconclusive (gray spheres). The lid of the ATP pocket is shown in green and ATP in natural colors.

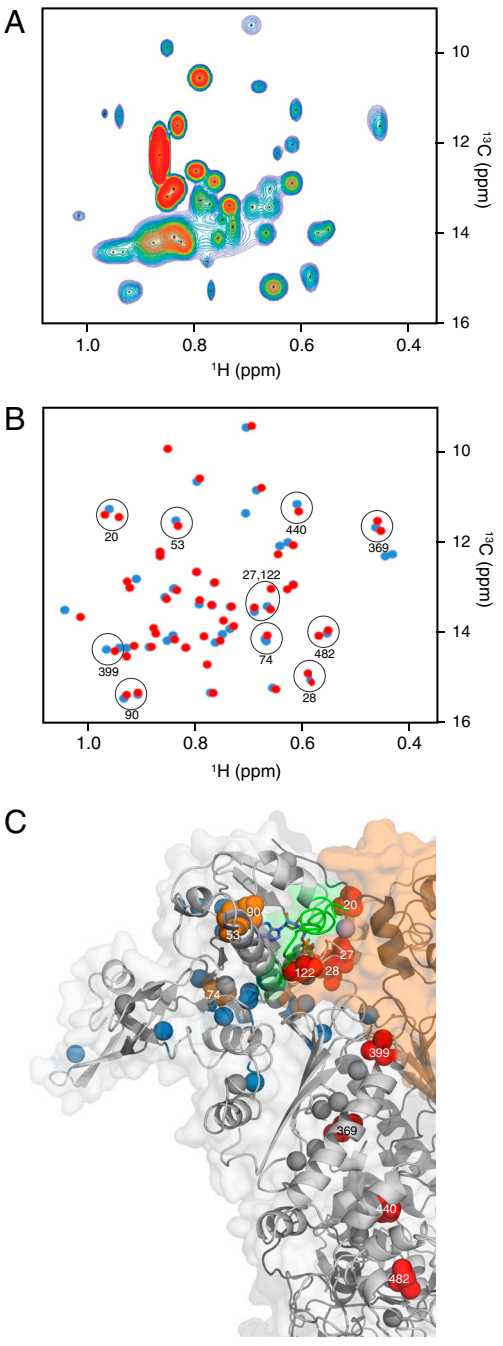

Fig. 3. The p23 binding site in Hsp90. (*A*) Rainbow representation of ^{1}H-^{13}C-Ile methyl-TROSY cross-peaks of full-length Hsp90 with ATP and p23 (120 μM Hsp90, 144 μM p23). The centers of 35 peaks are indicated by black dots. (*B*) Overlay of Hsp90 + ATP Ile methyl-TROSY spectra in absence (blue) and presence of p23 (red) shown as a peak position plot. The isoleucines showing significant shift are indicated and encircled (criteria as in Fig. 2*B*). (*C*) Ile side chains shifting upon p23 binding, plotted on one monomer of the model of the human Hsp90 structure. The color code is identical to Fig. 2*C*. p23 is shown semitransparent in orange.

indicated that the formation of stable Hsp90-p23 complexes required ATP. We did, therefore, the NMR analysis in the presence of ATP and the ATP-regenerating system. We observed p23-dependent shifts for a subset of peaks in both Hsp90-N and Hsp90-M (Fig. 3 *A* and *B* and Figs. S2*B* and S3*B*). In addition, we detected that some resonance signals were split into two peak components.

Most shifts in the N-terminal domain mapped to the lid over the ATP binding pocket and the layer beneath (including Ile20, Ile27, Ile28, and Ile122; Fig. 3*C*). Strikingly, p23-dependent perturbations reached out beyond the contact surfaces of the two p23 molecules identified in the crystal structure of the yeast

$Hsp90_2$-$Sba1^{p23}{}_2$ complex (11). We observed changes around Ile90 on the side of the ATP pocket that is distal from the lid segment. We conclude that p23 modulated the environment of the ATP binding pocket also at this end.

Surprisingly, we also detected shifts in residues spreading over large parts of Hsp90-M. The shifts included Ile399, corresponding to a known p23-binding surface in Hsp90-M (11). Most shifts in Hsp90-M, however, were distant from the expected p23-binding site (Ile369, Ile440, and Ile482). Those shifts indicate that in contrast to the ATP state, p23 induced long-range conformational changes in Hsp90-M.

It is controversial whether Hsp90 binds p23 at a 2:2 or 2:1 ratio (11–14). We found splitting for some peaks that could indicate asymmetry in the complex (Fig. 3*B*). To monitor the stoichiometry of the complex, we performed native mass spectrometry (27–29) of Hsp90 and p23 at various concentrations using comparable buffer conditions as in our NMR analysis (Fig. 4). At a 2:3 ratio of Hsp90 to p23 (monomer concentration) we observed next to some free $Hsp90_2$ primarily $Hsp90_2p23_2$, whereas only very little $Hsp90_2p23_1$ (Fig. 4*A*). These data point to a cooperative interaction of Hsp90 and p23 in the ratio used in the NMR experiments. The higher protein concentrations under NMR conditions would shift the equilibrium further to the 2:2 complex; thus $Hsp90_2p23_2$ was the dominant species in our NMR experiments (Fig. 3 *A* and *B*). Inside the cell, Hsp90 appears in excess over p23 (30). We also performed native mass spectrometry at 10-fold excess of Hsp90 to reflect the physiological ratio (Fig. 4*B*). We found that under those conditions both $Hsp90_2p23_1$ and $Hsp90_2p23_2$ are present in solution.

A particularly interesting conclusion can be drawn from comparing chemical shifts caused by ATP binding to Hsp90 with those of p23 binding to Hsp90-ATP. ATP binding does not cause any changes in Hsp90-M. In the presence of ATP, binding of p23 results in chemical shifts all over Hsp90-M, but this apparently extensive interaction was not sufficient to trigger p23 binding on its own in the absence of ATP. In the absence of ATP, p23 did not bind to Hsp90 (Fig. 4*C*), so it did not use the large interaction surface in Hsp90-M to form a stable complex. Interactions between the isolated middle domain and p23 have been observed in the absence of ATP, though (19). This leaves room for the interpretation that the N-terminal domain of Hsp90 may regulate binding of Hsp90 to p23 both positively and negatively. From all of the above we conclude that the N-terminal domain is the trigger factor for forming the Hsp90-p23 complex.

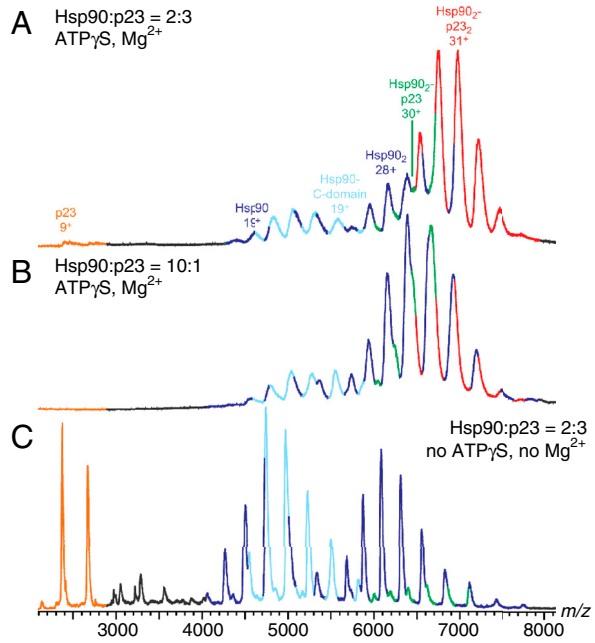

Fig. 4. Formation of $Hsp90_2p23_2$ is positively cooperative. Native mass spectra of Hsp90-p23 complexes, identified complexes are indicated by colors (p23, orange, Hsp90 monomer, purple; Hsp90–Hsp90-C, light blue; $Hsp90_2$, purple; $Hsp90_2$-p23, green; $Hsp90_2$-$p23_2$, red). (*A*) 2 μM Hsp90 and 3 μM p23, 1 mM MgOAc and 0.5 mM ATPγS. (*B*) 5 μM Hsp90 and 0.5 μM p23, 1 mM MgOAc and 0.5 mM ATPγS. (*C*) 2 μM Hsp90 and 3 μM p23, no ATP/Mg. We observed the following masses in absence of ATP and p23: Hsp90-C 19,340 ± 20 Da, p23 21,390 ± 20 Da, $Hsp90_1$ 85,200 ± 300 Da, Hsp90-Hsp90-C 104,600 ± 200 Da, $Hsp90_2$ 170,500 ± 200 Da, $Hsp90_2$-p23 192,000 ± 1,000 Da. In the presence of ATPγS, Mg^{2+} and p23 we observed the following: p23 21,490 ± 40 Da, $Hsp90_1$ 90,000 ± 3,000 Da, Hsp90-Hsp90-C 111,100 ± 400 Da, $Hsp90_2$ 174,000 ± 5,000 Da, $Hsp90_2$-p23 193,500 ± 200 Da, $Hsp90_2$-$p23_2$ 217,000 ± 3,000 Da.

Discussion

Our study adapted methyl-TROSY-based NMR spectroscopy to a large and rather complex molecule. Hsp90 is challenging for NMR for several reasons: (*i*) the large number of amino acids, (*ii*) the high molecular weight of 170 kDa for the Hsp90 dimer, (*iii*) the presence of significant dynamic segments besides rigid parts, (*iv*) potential symmetry breaks of the dimer, and (*v*) Hsp90 is too fragile to apply typically preferred NMR conditions such as very high protein concentration, low salt, and high temperature. Our data show that the technology pioneered by Kay and co-workers can be applied to such a complex molecule under almost physiological conditions (23, 31). The cellular Hsp90 concentration is between 10 and 150 μM, depending on the cell type, whereas we used 100 to 150 μM Hsp90 for the NMR experiments in this study (32). This opens the possibility to get insights into the active cycle of Hsp90 and its interactions with cofactors and offers a perspective to identify the substrate binding site. It also opens possibilities to analyze anticancer drugs that target Hsp90.

The Ile side chains are not evenly spread over Hsp90, most of them are in Hsp90-N (20 Iles, 12 of which could be unambiguously assigned in full-length Hsp90; Table S1). This makes the NMR analysis particularly sensitive for monitoring effects of nucleotides and inhibitors that bind to the N-terminal ATP binding pocket. Nevertheless, we could draw conclusions about ATP and p23 binding to Hsp90 without statistical bias due to varying content of Iles in the domains: We observed that none of the signals corresponding to residues of Hsp90-M or Hsp90-C shifted upon ATP binding, whereas four out of five Iles of Hsp90-M shifted unambiguously in the presence of both ATP and p23 (Fig. 2*C* and Fig. 3*C*).

We found that ATP binding does not induce conformational changes outside of the N-terminal domain (Fig. 2). The majority of the Hsp90 population would be open in our experiments, according to EM findings by the Agard group (10). This points to a simple regulatory mechanism of N-terminal dimerization, in which the positioning of the first helix of the N-terminal domain is crucial.

An increased ratio of open to closed conformation for human Hsp90 compared to other homologues requires more sophisticated regulation by cofactors. Our data indicate that p23 glues both halves of the human Hsp90 dimer together and interacts with the lid of the ATP binding pocket (Fig. 3), in pleasing congruence with previous crystallographic findings for the yeast homologues (11). This indicates that this step of the ATPase cycle is conserved between yeast and human Hsp90. We also find that p23 interacts with a large part of Hsp90-M (Fig. 3*C*), which agrees with the findings of a previous study analyzing the p23 interaction with Hsp90 fragments of various length (33).

The p23 protein is supposed to block the ATPase cycle by inhibiting the hydrolysis step. The mechanism of this step is enigmatic. This function is even surprising given that, in the case of the yeast homologue, $Sba1^{p23}$ was shown to position Hsp90 in the hydrolysis-competent conformation in the crystal structure (11). Together with our finding that p23 binding affects the lid

and the distal part of the nucleotide-binding pocket at Ile90 (Fig. 3*C*), we consider that p23 may change the environment of the nucleotide. Those changes might be mediated either through the protein and/or via the nucleotide and may allow for a p23-mediated mechanism to slow down the ATPase cycle. We noted that the position of inhibitors and nucleotides is identical in several crystal structures of Hsp90-N fragments. Hsp90 is a member of the GHKL ATPase family, which all share the same architecture of the ATP binding pocket. Interestingly, the ATP molecule in the GHKL protein MutL is pushed by 1.7 Å to its distal end, compared to the Hsp90 structures (Fig. S5*B*), whereas the homologous turn that would correspond to Ile90 is pushed back by 2.2 Å (34). We also see in solution upon p23 binding extensive changes in the middle domain, more extensive than expected before, which might have a bearing on the positioning of the catalytic Arg391 (Fig. 3*C*). Together, those results indicate that p23's interaction with Hsp90 is a rather intimate affair.

Our data are in agreement with earlier findings that the human Hsp90 dimer preferentially binds two p23 molecules (13, 35). ITC studies for the yeast homologues found either only one $Sba1^{p23}$ bound to Hsp90 or an anticooperative effect (12, 14). Our native mass spectrometry-based analysis suggests a cooperative effect for the human homologue (Fig. 4). The cellular concentration of Hsp90 is one order of magnitude above that of p23, which would otherwise favor $Hsp90_2p23_1$ complexes (30). Positive cooperativity will be vital to ensure binding of two p23 to human Hsp90 under physiological conditions.

Based on data presented here and results of others, we summarize the Hsp90-p23 association in five steps and conclude that the key trigger for this interaction is in the N-terminal domain (Fig. 5): (*i*) ATP binds to both N-terminal domains of the Hsp90 dimer, (*ii*) Hsp90's N-terminal domains transiently dimerize into the closed conformation in equilibrium with the open state, (*iii*) binding of p23 to both N-terminal domains of the Hsp90 dimer links both halves of the molecule, (*iv*) contacts with the middle domain stabilize the interaction with p23; those contacts support p23's interaction but are not sufficient to induce binding to Hsp90 in the absence of ATP, and (*v*) binding of the second p23 to the other side of Hsp90; this cooperative interaction is supported by the association of the N-terminal domains in the Hsp90 dimer, which was already induced by binding of the first p23 molecule.

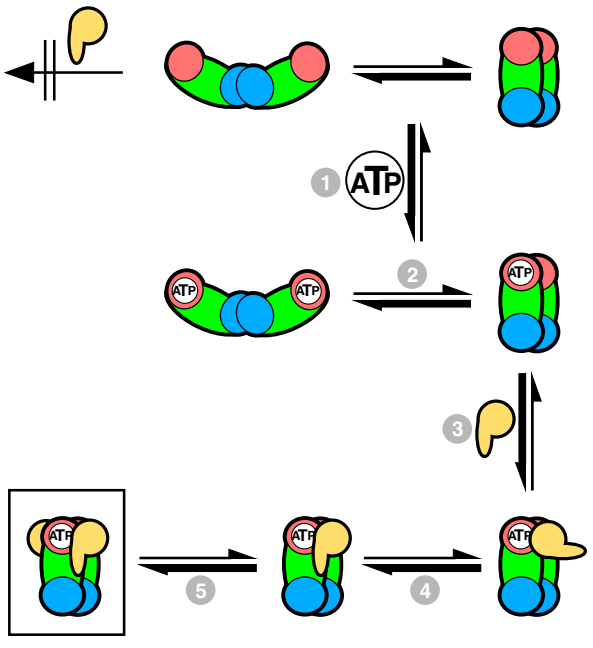

Fig. 5. The N-terminal domain of Hsp90 triggers p23 binding. Both Apo and ATP-bound human Hsp90 (Hsp90-N, red; Hsp90-M, green; Hsp90-C, blue) are predominantly open under equilibrium conditions (10). p23 (orange) cannot bind to Apo Hsp90, indicating that the interactions with Hsp90-M are not sufficient for binding. p23 can bind to Hsp90 after dimerization of the N-terminal domains are achieved, allowing for strengthening of the interaction by contacts with Hsp90-M. Afterward, a second p23 molecule binds, resulting in a $Hsp90_2p23_2$ complex (boxed). The steps of the Hsp90-p23 association are indicated by numbers 1–5, as described in the text.

Most of the key cofactors of Hsp90 were shown to be part of asymmetric Hsp90 complexes, including $Cdc37^{p50}$, Aha1, CHIP, and Sgt1 (17, 36–39). Formation of 2:1 complexes with an otherwise symmetric dimer is rare, and we speculate that this might be related to the order in which the two halves of the Hsp90 dimer hydrolyze ATP. In that light it is surprising that p23 would bind in 2:2 stoichiometry to Hsp90. It has not escaped our notice, though, that the splitting of a subset of peaks in our NMR spectra of Hsp90-p23 complexes might reflect asymmetry in an Hsp90-p23 complex with symmetric stoichiometry.

In this study, we characterized structural properties of full-length Hsp90 by NMR spectroscopy using methyl-specific labeling techniques. It allowed us to analyze the Apo, ATP, and ATP-p23 bound states in solution under identical buffer conditions. Such techniques had been successfully applied to monitor conformational changes in the proteasome and the interaction of the SecA translocase with a signal peptide (24, 40, 41). Our study demonstrates that this technology can be applied to monitor conformational changes in large heterogeneous proteins that contain both flexible and rigid parts. We expect that this study will be the basis for analyzing Hsp90's interaction with cochaperones, protein substrates and drugs in solution.

Methods

Expression and Purification. All proteins were produced with N-terminal his tag. Cells expressing human Hsp90β and its domains (Hsp90 full length, residues P1-D723; Hsp90-N, P1-E233; Hsp90-M, S260-K551; Hsp90-C, E546-D723) were grown in either 99% D_2O or H_2O minimal medium containing $^{15}NH_4Cl$ as the sole nitrogen source and $^{1}H/^{12}C$, $^{2}H/^{12}C$, or $^{2}H/^{13}C$ glucose as the carbon source. To achieve methyl labeling, the media were supplemented with 100 mg/L 2-keto-3,3-d2-4-^{13}C-butyrate (for Ile-[δ1-$^{13}CH_3$]) 1 h prior to protein induction, modified from ref. 42. All proteins were purified on Poros 20MC metal chelate media followed by Poros 20HQ anion exchange media. Human p23 was expressed in D_2O-M9 media and purified as described for Hsp90.

NMR Spectroscopy. ^{1}H-^{13}C-methyl-TROSY spectra (42) were recorded at 25 °C on a Bruker AvanceII 900-MHz spectrometer equipped with a TCI cryoprobe. Reported chemical shifts are referenced against 2,2-dimethyl-2-silapentane-5-sulfonic acid. For the backbone resonance assignment of the apo Hsp90-N and Hsp90-M TROSY variants of the triple-resonance experiments HNCO, HN(CA)CO, HNCA, HNCACB, and HNCOCACB (31, 32) assignment were recorded using [U-^{13}C,^{15}N,^{2}H] labeled samples in protonated water buffer. Assignments were supplemented with ^{15}N-^{1}H 2D TROSY, ^{13}C-resolved 3D CC TOCSY, and ^{15}N-resolved 3D NOESY experiments. For the AMP-PNP (2 mM, Sigma) bound form of the Hsp90-N another series of triple-resonance spectra was required, because AMP-PNP binds Hsp90 in the slow exchange regime on the NMR time scale leading to an additional set of signals. HCcH and hCCH 3D TOCSY spectra were recorded on additional samples of [U-^{13}C,^{15}N] labeled Hsp90-N and Hsp90-M to correlate side chain proton and carbon resonances of Ile s to the available backbone assignments of Cα and Cβ from the deuterated protein samples. Cα and Cβ backbone chemical shifts were corrected for the deuterium isotope effect to match the carbon chemical shifts derived from the HCCH TOCSY's.

All spectra were processed with TopSpin (Bruker). Spectral analysis and peak picking was performed with Sparky (T. D. Goddard and D. G. Keller, SPARKY 3, University of California, San Francisco). Peak position plots were drawn using the chemical shift values (^{13}C and ^{1}H) for each Ile residue. The sequential backbone assignment was carried out using the triple-resonance NMR spectra in combination with PACES (43). The cross-peaks of the methyl-TROSY spectra were 2D-line shape fitted using mixed Lorentzian/Gaussian deconvolution parameters (TopSpin). Rainbow representations were done by overlaying 14 spectra with linearly increasing the lowest contour level. Each increment was determined by subtracting the lowest contour level from

the intensity of the peak corresponding to Ile174, considered as the reference peak.

NMR samples of Hsp90 contained between 100 and 250 μM Hsp90 in 100% D_2O, 25 mM sodium phosphate, pH 7.2, 300 mM NaCl, 1 mM TCEP. Spectra of Hsp90-p23 complexes were acquired with 100–120 μM Hsp90 and were titrated with 0.5 to 2 M equivalents of p23 (monomer concentrations) using an ATP-regenerating system consisting of 50 units of creatine phosphokinase, 20 mM creatine phosphate, 2.5 mM ATP, and 5 mM $MgSO_4$.

Homology Modeling. The structure of human Hsp90β is a homology model calculated with SWISS-MODEL using as template the structure of yeast Hsp90 PDB ID code 2CG9 (44). The molecular structures were generated using Pymol (PyMOL Molecular Graphics System, Schrödinger, LLC).

Native Mass Spectrometry. Electrospray ionization (ESI) mass spectrometry measurements were performed on a modified QTOF 2 (Waters/MS Visions) (45) operated in positive ion mode. To achieve optimal resolution the backing pressure was increased to 10 mbar. The capillary and cone voltages were 1,300 V and 150 V, respectively. Pressure in the collision cell was $1.5\ 10^{-2}$ mbar with xenon as collision gas (46) where the acceleration voltage was 50 V. Capillaries for ESI were prepared in house from borosilicate glass tubes of 1.2 mm OD and 0.68 mm ID with filament (World Precision Instruments) using a P-97 micropipette puller (Sutter Instruments) and gold-coated using an Edwards Scancoat (Edwards Laboratories) six Pirani 501 sputter coater. Capillary tips were opened on the sample cone of the instrument.

Buffer exchange to 50–300 mM NH_4OAc, pH 7.2, and 1 mM DTT for Hsp90 and p23 was carried out using centrifugal filter units at $15{,}000 \times g$, 4 °C (5-kDa cutoff, Vivaspin 500, Sartorius AG). Hsp90 (2 to 5 μM) was mixed with p23 (0.5 to 5 μM) in presence and absence of 1 mM MgOAc and 0.5 mM ATPγS followed by 1-h incubation at 30 °C prior to mass spectrometric analysis.

Mass spectra were calibrated where necessary with cesium iodide and analyzed using Masslynx and ESIprot (47). The assigned complex stoichiometries were verified in tandem mass spectrometry experiments. The increase of detected relative to calculated m/z results from involatile buffer compounds sticking to the complex, especially ATPγS and Mg (see also Fig. 4 *B* and *C*). In addition to the expected peaks, we identified a peak that referred to a dimeric peak of Hsp90 with Hsp90-C, which was present in minor amounts in all analyzed Hsp90 samples, also in absence of p23. Hsp90 is known to be sensitive to proteolytic processing at the hinges between domains.

ACKNOWLEDGMENTS. We are grateful to Ineke Braakman for continuous support and critical comments throughout this study. We thank Eric Huizinga for valuable discussions and structural insights and Stefan Freund, Assaf Friedler, and Chris Prodromou for comments on the manuscript. We thank Mariëtte van Eck for experiments. The p23 expression plasmid was the kind gift of Matthias P. Mayer (Heidelberg University, Heidelberg, Germany). S.G.D.R. was supported by a Marie-Curie Excellence Grant of the European Union, a VIDI career development grant by the Netherlands Organization for Scientific Research (NWO) and a High Potential Grant of Utrecht University. R.B. was supported by NWO-Chemical Sciences (NWO-CW) for the 900 MHz NMR and the TCI cryoprobe.

1. Pearl LH, Prodromou C (2006) Structure and mechanism of the hsp90 molecular chaperone machinery. *Annu Rev Biochem* 75:271–294.
2. Wandinger SK, Richter K, Buchner J (2008) The Hsp90 chaperone machinery. *J Biol Chem* 283:18473–18477.
3. Richter K, Buchner J (2006) Hsp90: Twist and fold. *Cell* 127:251–253.
4. Krukenberg KA, Forster F, Rice LM, Sali A, Agard DA (2008) Multiple conformations of E. coli Hsp90 in solution: Insights into the conformational dynamics of Hsp90. *Structure* 16:755–765.
5. Graf C, Stankiewicz M, Kramer G, Mayer MP (2009) Spatially and kinetically resolved changes in the conformational dynamics of the Hsp90 chaperone machine. *EMBO J* 28:602–613.
6. Dollins DE, Warren JJ, Immormino RM, Gewirth DT (2007) Structures of GRP94-nucleotide complexes reveal mechanistic differences between the hsp90 chaperones. *Mol Cell* 28:41–56.
7. Bron P, et al. (2008) Apo-Hsp90 coexists in two open conformational states in solution. *Biol Cell* 100:413–425.
8. Hessling M, Richter K, Buchner J (2009) Dissection of the ATP-induced conformational cycle of the molecular chaperone Hsp90. *Nat Struct Mol Biol* 16:287–293.
9. Mickler M, Hessling M, Ratzke C, Buchner J, Hugel T (2009) The large conformational changes of Hsp90 are only weakly coupled to ATP hydrolysis. *Nat Struct Mol Biol* 16:281–286.
10. Southworth DR, Agard DA (2008) Species-dependent ensembles of conserved conformational states define the Hsp90 chaperone ATPase cycle. *Mol Cell* 32:631–640.
11. Ali MM, et al. (2006) Crystal structure of an Hsp90-nucleotide-p23/Sba1 closed chaperone complex. *Nature* 440:1013–1017.
12. Siligardi G, et al. (2004) Co-chaperone regulation of conformational switching in the Hsp90 ATPase cycle. *J Biol Chem* 279:51989–51998.
13. McLaughlin SH, et al. (2006) The co-chaperone p23 arrests the Hsp90 ATPase cycle to trap client proteins. *J Mol Biol* 356:746–758.
14. Richter K, Walter S, Buchner J (2004) The co-chaperone Sba1 connects the ATPase reaction of Hsp90 to the progression of the chaperone cycle. *J Mol Biol* 342:1403–1413.
15. Bertelsen EB, Chang L, Gestwicki JE, Zuiderweg ER (2009) Solution conformation of wild-type *E. coli* Hsp70 (DnaK) chaperone complexed with ADP and substrate. *Proc Natl Acad Sci USA* 106:8471–8476.
16. Revington M, Zhang Y, Yip GN, Kurochkin AV, Zuiderweg ER (2005) NMR investigations of allosteric processes in a two-domain thermus thermophilus Hsp70 molecular chaperone. *J Mol Biol* 349:163–183.
17. Retzlaff M, et al. (2010) Asymmetric activation of the Hsp90 dimer by its cochaperone Aha1. *Mol Cell* 37:344–354.
18. Dehner A, et al. (2003) NMR chemical shift perturbation study of the N-terminal domain of Hsp90 upon binding of ADP, AMP-PNP, geldanamycin, and radicicol. *ChemBioChem* 4:870–877.
19. Martinez-Yamout MA, et al. (2006) Localization of sites of interaction between p23 and Hsp90 in solution. *J Biol Chem* 281:14457–14464.
20. Sreeramulu S, et al. (2009) The human Cdc37·Hsp90 complex studied by heteronuclear NMR spectroscopy. *J Biol Chem* 284:3885–3896.
21. Jacobs DM, et al. (2006) NMR backbone assignment of the N-terminal domain of human HSP90. *J Biomol NMR* 36(Suppl 1):52.
22. Rüdiger S, Freund SM, Veprintsev DB, Fersht AR (2002) CRINEPT-TROSY NMR reveals p53 core domain bound in an unfolded form to the chaperone Hsp90. *Proc Natl Acad Sci USA* 99:11085–11090.
23. Tugarinov V, Hwang PM, Ollerenshaw JE, Kay LE (2003) Cross-correlated relaxation enhanced ^{1}H-^{13}C NMR spectroscopy of methyl groups in very high molecular weight proteins and protein complexes. *J Am Chem Soc* 125:10420–10428.
24. Sprangers R, Kay LE (2007) Quantitative dynamics and binding studies of the 20S proteasome by NMR. *Nature* 445:618–622.
25. McLaughlin SH, Ventouras LA, Lobbezoo B, Jackson SE (2004) Independent ATPase activity of Hsp90 subunits creates a flexible assembly platform. *J Mol Biol* 344:813–826.
26. Stebbins CE, et al. (1997) Crystal structure of an Hsp90-geldanamycin complex: Targeting of a protein chaperone by an antitumor agent. *Cell* 89:239–250.
27. Heck AJ (2008) Native mass spectrometry: A bridge between interactomics and structural biology. *Nat Methods* 5:927–933.
28. Heck AJ, Van Den Heuvel RH (2004) Investigation of intact protein complexes by mass spectrometry. *Mass Spectrom Rev* 23:368–389.
29. Benesch JL, Ruotolo BT, Simmons DA, Robinson CV (2007) Protein complexes in the gas phase: Technology for structural genomics and proteomics. *Chem Rev* 107:3544–3567.
30. Picard D (2006) Intracellular dynamics of the Hsp90 co-chaperone p23 is dictated by Hsp90. *Exp Cell Res* 312:198–204.
31. Sprangers R, et al. (2008) TROSY-based NMR evidence for a novel class of 20S proteasome inhibitors. *Biochemistry* 47:6727–6734.
32. Nollen EA, Morimoto RI (2002) Chaperoning signaling pathways: Molecular chaperones as stress-sensing 'heat shock' proteins. *J Cell Sci* 115:2809–2816.
33. Chadli A, et al. (2000) Dimerization and N-terminal domain proximity underlie the function of the molecular chaperone heat shock protein 90. *Proc Natl Acad Sci USA* 97:12524–12529.
34. Ban C, Junop M, Yang W (1999) Transformation of MutL by ATP binding and hydrolysis: A switch in DNA mismatch repair. *Cell* 97:85–97.
35. Phillips JJ, et al. (2007) Conformational dynamics of the molecular chaperone Hsp90 in complexes with a co-chaperone and anticancer drugs. *J Mol Biol* 372:1189–1203.
36. Zhang M, et al. (2005) Chaperoned ubiquitylation—crystal structures of the CHIP U box E3 ubiquitin ligase and a CHIP-Ubc13-Uev1a complex. *Mol Cell* 20:525–538.
37. Zhang M, et al. (2008) Structural and functional coupling of Hsp90- and Sgt1-centred multi-protein complexes. *EMBO J* 27:2789–2798.
38. Vaughan CK, et al. (2006) Structure of an Hsp90-Cdc37-Cdk4 complex. *Mol Cell* 23:697–707.
39. Zhang M, Kadota Y, Prodromou C, Shirasu K, Pearl LH (2010) Structural basis for assembly of Hsp90-Sgt1-CHORD protein complexes: Implications for chaperoning of NLR innate immunity receptors. *Mol Cell* 39:269–281.
40. Religa TL, Sprangers R, Kay LE (2010) Dynamic regulation of archaeal proteasome gate opening as studied by TROSY NMR. *Science* 328:98–102.
41. Gelis I, et al. (2007) Structural basis for signal-sequence recognition by the translocase motor SecA as determined by NMR. *Cell* 131:756–769.
42. Tugarinov V, Hwang PM, Kay LE (2004) Nuclear magnetic resonance spectroscopy of high-molecular-weight proteins. *Annu Rev Biochem* 73:107–146.
43. Coggins BE, Zhou P (2003) PACES: Protein sequential assignment by computer-assisted exhaustive search. *J Biomol NMR* 26:93–111.
44. Arnold K, Bordoli L, Kopp J, Schwede T (2006) The SWISS-MODEL workspace: A web-based environment for protein structure homology modelling. *Bioinformatics* 22:195–201.
45. van den Heuvel RH, et al. (2006) Improving the performance of a quadrupole time-of-flight instrument for macromolecular mass spectrometry. *Anal Chem* 78:7473–7483.
46. Lorenzen K, Versluis C, van Duijn E, van den Heuvel RHH, Heck AJR (2007) Optimizing macromolecular tandem mass spectrometry of large non-covalent complexes using heavy collision gases. *Int J Mass Spectrom* 268:198–206.
47. Winkler R (2010) ESIprot: A universal tool for charge state determination and molecular weight calculation of proteins from electrospray ionization mass spectrometry data. *Rapid Commun Mass Spectrom* 24:285–294.